

Life-cycle cost evaluation of steel structures retrofitted with steel slit damper and shape memory alloy-based hybrid damper

Advances in Structural Engineering
2019, Vol. 22(1) 3–16
© The Author(s) 2018
Article reuse guidelines:
sagepub.com/journals-permissions
DOI: 10.1177/1369433218773487
journals.sagepub.com/home/ase



Mohamed NourEldin, Asad Naeem and Jinkoo Kim

Abstract

In this study, the seismic capacity of a hybrid damper, composed of a steel slit plate damper and two shape memory alloy bars, is investigated through fragility analysis and life-cycle cost evaluation of a steel frame retrofitted with the damper. The nonlinear time history analysis model frames show that the seismic responses of the frames equipped with hybrid damper are significantly lesser than the frames retrofitted with conventional slit dampers. The enhancement in the seismic performance of frames retrofitted with hybrid damper is because of extra stiffness, energy dissipation, and self-centering capability provided by the shape memory alloy bars. It is also observed that the life-cycle cost of the frames equipped with hybrid dampers is smallest compared with the life-cycle cost of the bare frames and the frames equipped with slit dampers, even though the initial cost of the hybrid damper is higher than that of the conventional slit damper.

Keywords

life-cycle cost, seismic retrofit, self-centering capability, shape memory alloy, slit dampers, superelastic effect

Introduction

Recently, various energy dissipation devices have been developed and used for seismic protection of existing structures. Researchers are trying to investigate the simultaneous application of multiple damping devices to maximize the energy dissipation mechanism with higher efficiency. For example, Tsai et al. (1998), Pong et al. (2002), and Uetani et al. (2003) studied combined displacement-dependent and velocity-dependent devices for seismic mitigation of structures to minimize the shortcomings of individual conventional dampers. Marshall and Charney (2012) studied a hybrid system with buckling-restrained braces (BRBs) and viscous fluid device by investigating the seismic response of steel frame structures. Lee and Kim (2015) carried out seismic performance evaluation of moment frames with hybrid dampers (HDs) in which a steel slit plate and a friction damper are connected in parallel. Salari and Asgarian (2015) investigated seismic response of steel braced frames equipped with hybrid devices composed of shape memory alloy (SMA) wires and steel pipes and showed that the hybrid device has a considerable potential to mitigate the residual drift ratio, peak absolute acceleration, and peak interstory drift of the structure. Zhu and Zhang (2008) proposed self-

centering friction damping brace system using Nitinol wires (SMA) and showed that the proposed braces can achieve a seismic response level similar to BRB. The design procedure and the shake-table test result of steel structure retrofitted with self-centering SMA system are shown in Qiu and Zhu (2017). Kim and Shin (2017) conducted a cyclic loading test and seismic loss assessment of a structure retrofitted with slit-friction hybrid dampers. The results of the previous studies demonstrate the capability of HDs to improve structural response compared with conventional dampers. The hybrid configuration improved stiffness, ductility, and strength of the structural system, providing benefits for multiple damage measures.

In seismic engineering, life-cycle cost (LCC) analysis is considered as one of the effective tools for quantitative risk analysis which explicitly considers the

Department of Civil and Architectural Engineering, Sungkyunkwan University, Suwon, Republic of Korea

Corresponding author:

Jinkoo Kim, Department of Civil and Architectural Engineering, Sungkyunkwan University, (16419) 2066, Seobu-Ro, Jangan-Gu, Suwon-Si, Gyeonggi-Do, Korea.
Email: jkim12@skku.edu

consequences of earthquake events in terms of seismic induced losses. Previously, LCC analysis is mostly used to achieve optimal designs of different types of structure and seismic risk mitigation decision. Gencturk (2013) focused on life-cycle cost analysis of reinforced concrete (RC) and engineered cementitious composite frames. Taflanidis and Gidaris (2013) presented a systematic probabilistic framework for detailed estimation and optimization of LCC of passive dissipative devices in building structural system for seismic risk mitigation. They also studied the probabilistic approaches for comprehensive cost-effective design of viscous dampers based on LCC. Shin and Singh (2014) developed an approach to calculate the failure and life-cycle costs associated with different levels of damage considering the random occurrences of seismic events and uncertainties in the calculated response. A simplified method of collapse fragility and relations between equivalent single-degree-of-freedom characteristics and multi-degree-of-freedom story drift and floor acceleration for building structures is provided in Sullivan et al. (2014). Li et al. (2009) and NourEldin and Kim (2016) conducted LCC evaluation of offshore platforms.

SMA is relatively new material in the field of the seismic retrofit of structures. The superelastic effect of SMA is expected to reduce LCC of the structure after an earthquake when it is incorporated with conventional passive dampers. Ocel et al. (2004) presented a new steel beam–column connection using SMAs. Ma and Cho (2008) presented a re-centering SMA damper which consists of two groups of SMA wires and two springs, functioning as energy dissipating and re-centering groups, respectively, and the numerical simulation results showed that the SMA damper could reduce the residual deformation of the structure effectively. SMA was also applied to cross-bracing cables (McCormick et al., 2007), fiber reinforced polymer (FRP) composite reinforcements (Wierschem and Andrawes, 2010), RC beam–column joints (2011), BRBs (Miller et al., 2012), bridge cables (Torra et al., 2014), passive control devices (Han et al., 2006; Jalaeefar and Asgarian, 2014), motion control devices (Nakshatharan et al., 2014), seismic isolators (Ozbulut and Silwal, 2016), steel re-bars (Mirtaheeri et al., 2017), and retrofit of structures (Rameshwar, 2014). These studies show that utilizing SMA can improve the seismic performance of structures by providing the re-centering capability.

The literature review reveals that limited studies have been conducted on the LCC of building structures retrofitted with energy dissipation devices made of SMA. The objective of the current study is to investigate the seismic performance of structures with HDs

composed of steel slit dampers (SDs) and SMA bars developed by Naeem et al. (2017). The LCC is evaluated using full fragility curve, obtained from complete rigorous incremental dynamic analysis, and the results are compared to the simplified LCC methodology using an approximate fragility curve (AFC).

Nonlinear modeling of the HDs

Steel SDs have been applied to structures as effective and economic seismic retrofit devices (Kim and Shin, 2017; Saffari et al., 2013). However, the shortcoming of the hysteretic SDs is that the structure may have permanent deformation after experiencing an earthquake. In this study, HD developed using a conventional steel SD incorporated with SMA bars has been investigated using fragility analysis and LCC. The HD dissipates seismic energy efficiently by yielding of steel slit strips, and self-centering force is provided by the superelastic property of the SMA bars installed diagonally on both faces of the steel SD. The SMA bars are connected to the steel slit plate at both ends using anchorage and bolts. It is assumed in the analysis modeling that the SMA bars do not resist compression. The bars are installed diagonally in X shape so that at least one SMA bar is subjected to tension during cyclic motion, while the other SMA bar experiences compression which can slide through the anchorage. The HD with SMA bars is shown in Figure 1(a), and Figure 1(b) shows the installation scheme of the HD.

The steel SD used in the HD is composed of nine vertical strips, as shown in Figure 2. The in-plane stiffness of the SD can be obtained as follows (Chan and Albermani, 2008) based on the assumption that both ends of the strips are rigidly connected to the steel plate

$$K = n \frac{12EI}{l_0} = n \frac{Et b^3}{l_0} \quad (1)$$

where n is the number of the prismatic strips, t is the thickness of the strips, b is the width of the strips, and l_0 is the length of the strip.

Plastic hinges form at both ends of the strip with the full plastic moment (equation (2)) obtained as the product of the yield stress σ_y and the plastic section modulus

$$M_p = \sigma_y \frac{t b^2}{4} \quad (2)$$

The yield load of the SD, P_y , can be defined by the plastic bending mechanism with the assumption of perfectly elasto-plastic material behavior (Chan and Albermani, 2008)

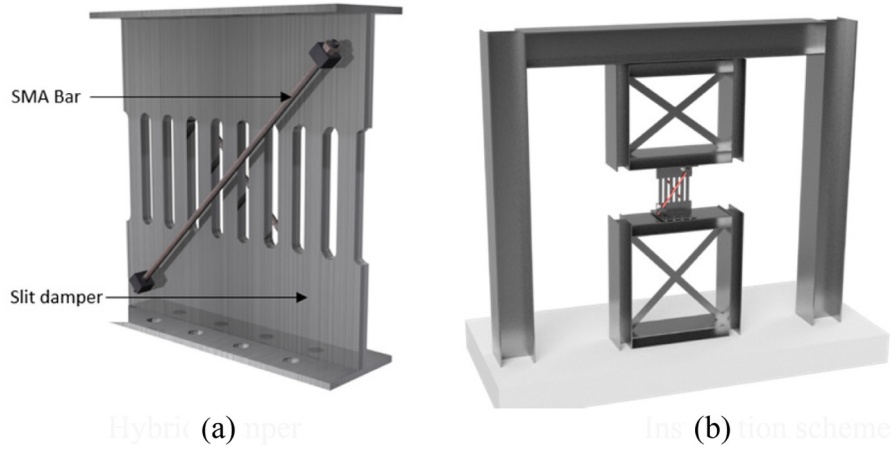


Figure 1. Configuration of the steel slit-SMA hybrid damper: (a) hybrid damper and (b) installation scheme.

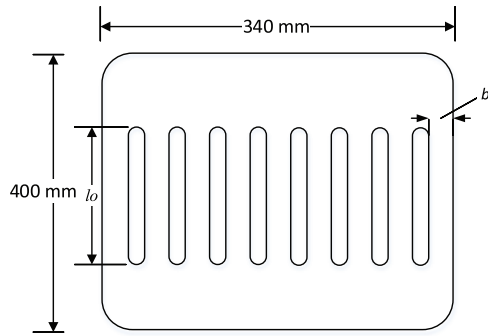


Figure 2. Size of the slit damper used in the analysis.

$$P_y = \frac{2nM_p}{l_0} = \sigma_y \frac{ntb^2}{2l_0} \quad (3)$$

The yield stress of the SD used in this study is 325 MPa, the thickness of the strip t is 20 mm, the width of the strip b is 20 mm, the length of the slit l_0 is 200 mm, and the number of strip n is 9. These values produce the yield strength and stiffness of the SD of 58 kN and 36.9 kN/mm, respectively.

The combined behavior of the HD can be obtained by superimposing superelastic behavior of SMA and the elasto-plastic behavior of the SD. The stiffness of the HD can be calculated using equation (4). The total force of the HD can be determined by adding together component forces at the corresponding displacement (Δ), as shown in Figure 3, which depicts the force–deformation relation of the HD

$$K = n \frac{Etb^3}{l_0} + \frac{AE}{L} \quad (4)$$

The amount of permanent deformation in the HD is dependent on the self-centering force regulated by

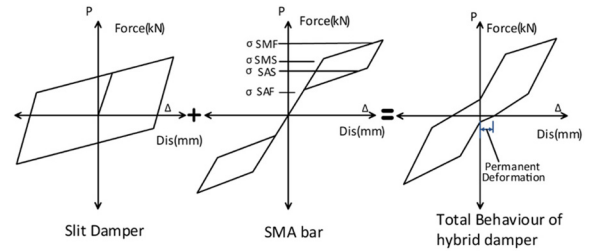


Figure 3. Idealized force–deformation relation of the hybrid damper (not to scale).

the size and material properties of the superelastic SMA bars. Material properties of the SMA bars with 10 mm diameter and length of 450 mm are as follows: elastic modulus = 80 GPa, Poisson's ratio = 0.33, martensite start stress (σ_{SMS}) = 440 MPa, martensite finish stress (σ_{SMF}) = 540 MPa, austenite start stress (σ_{SAS}) = 250 MPa, austenite finish stress (σ_{FAS}) = 140 MPa. With this information, the yield strength and initial stiffness of the HD are 130 kN and 80 kN/mm, respectively, which are approximately twice compared to the SD without the SMA bars.

The behavior of the HD is modeled using nonlinear link elements provided in the SAP2000 software. To model the superelastic behavior of SMA bar, a hook and a gap link are connected in series with a multi-linear plastic (MLP) link as shown in Figure 4(a). They are connected in parallel with two multi-linear elastic links (MLE1 and MLE2). These links are connected in series with a linear link (LIN1). The SD is modeled as a plastic link element. It is observed in the preliminary analysis that the arrangement of the various link elements, as shown in Figure 4(a), can accurately express the self-centering behavior of the SMA bar. Figure 4(b) depicts the one complete cycle of the

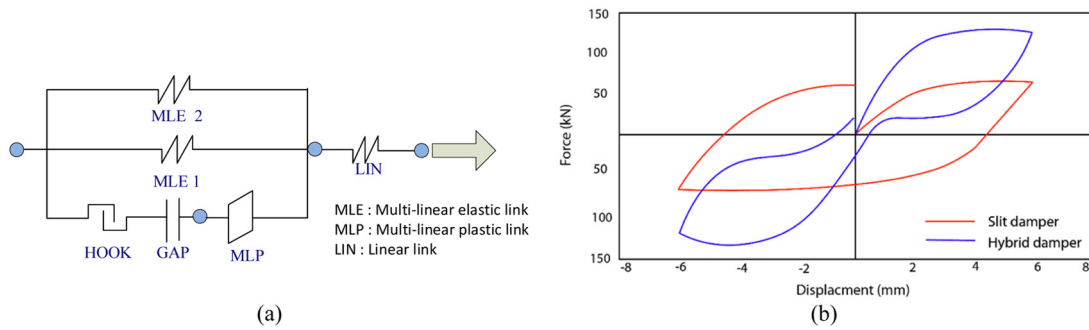


Figure 4. (a) Link element model for hybrid damper and (b) force–deformation relation of the hybrid damper.

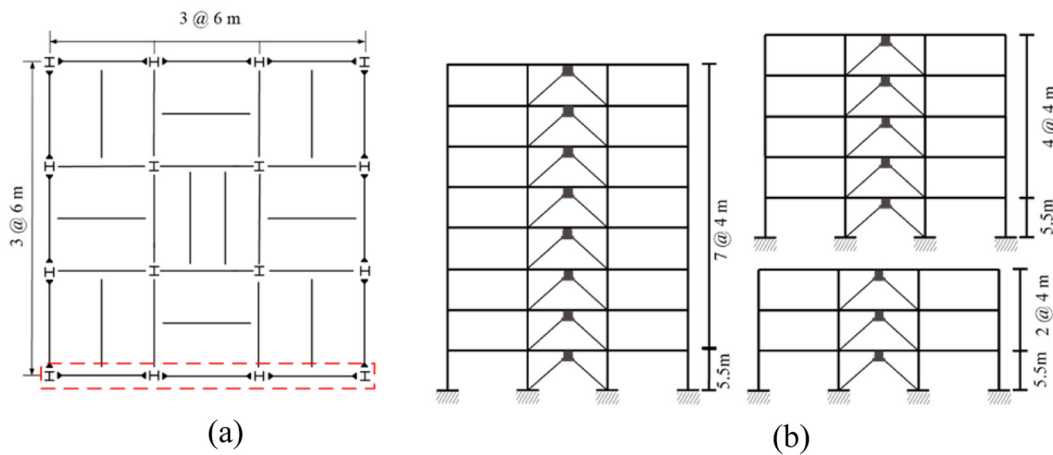


Figure 5. Analysis model structures: (a) structural plan and (b) elevation of structures with damper.

force–deformation curve of the HD and the SD used in the analysis. Further more details about the modeling of SMA can be found elsewhere (Naeem et al., 2017)

Seismic performance evaluation

Design of the prototype structures

To investigate the seismic performance of HD, three conventional three-story, five-story, and eight-story steel structures are taken as prototype structures. The steel structures are ordinary moment resisting frames (OMRF) designed using gravity loads only. Each prototype structures have story height of 4000 and 5500 mm for the first story. The span length is 6000 mm in both directions. The plan and elevation of the prototype structures are shown in Figure 5, and only one of the exterior frame is separated for the analysis; the position of the dampers is also shown in Figure 5(b). The design dead and live loads are 4.1 and 2.5 kN/m², respectively. Beam and column of both the

structures are W-shaped sections. The material properties of steel A-36 (ASTM) with a yield stress of 250 MPa are used for beams and A-572 (ASTM) with a yield stress of 345 MPa is used for columns. Figure 6 shows the stress–strain relationship of the materials.

To carry out nonlinear dynamic analysis of the model structures, the material model of the structural members recommended by the FEMA 356 (2000) is used. Plastic hinges are introduced at the end of columns and beams; to account for the inelastic activity of the members, Figure 7(a) shows the bending moment versus rotation angle relationship of the flexural members. The coefficients used to define the nonlinear behavior (a , b , and c) are computed considering the width–thickness ratios of the structural members and are summarized in Table 1, for each of the model structures. Figure 7(b) indicates the deformation levels corresponding to each performance point such as the first yield, immediate occupancy (IO), life safety (LS), collapse prevention (CP), collapse, and fracture specified in the FEMA 356 (2000). The inherent damping ratio of the structure is assumed to be 3% of the critical damping.

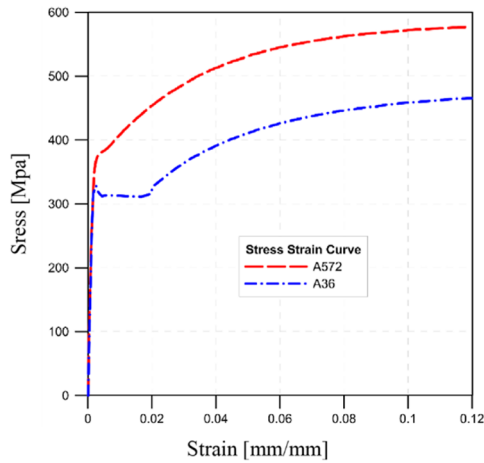


Figure 6. Stress–strain relationship of steel material.

Nonlinear dynamic analysis results

The seismic performance of the model structures is analyzed using the software SAP2000 (Computer and Structure Inc., 2010). The bending moment–rotation relationships of the beams and columns are set up as shown above. A modal damping ratio of 5% of the critical damping is used in the dynamic analysis of the model structures. The seismic load used for seismic performance evaluation of the prototype structures is computed based on the design spectral acceleration parameters $S_{DS} = 1.46$ and $S_{D1} = 0.737$. This corresponds to the design seismic load for buildings in Los Angeles area with site class “D”.

Figure 8 shows the nonlinear static pushover analysis results of the bare frame (BF) and the frames retrofitted with the SD and the HD. The comparison of pushover curves of the frames shows that strength and

Table 1. Coefficients for defining nonlinear behavior of flexural members.

Span	Story	Parameters		
		<i>a</i>	<i>b</i>	<i>c</i>
6 m	3 and 8	9	11	0.6

stiffness of the structures are increased after the installation of the damper. The frame retrofitted with the HD shows much larger strength and ductility compared to the frame retrofitted with SD. The prototype frames are subjected to three set of ground motion scaled to the design basis level earthquake response spectrum of Los Angeles. The earthquake used for the nonlinear time history analysis is shown in Table 2. The results are compared to BF, frame retrofitted with SD, and frame retrofitted with HD.

Figure 9 shows the time history roof displacement of the five-story frame. It can be observed that the roof displacements decrease significantly for the frame retrofitted with HD and SD. However, frame equipped with the HD experiences least residual deformation, compared to the BF and the frame retrofitted with the SD. Figure 10 shows the maximum interstory drift ratio (MIDR) for the BF, frame with SD, and frame equipped with HD for the three individual ground motions. It can be observed that the mean MIDR for a frame equipped with the HD turned out to be lowest with 0.45%. But for the SD-retrofitted frame and the BF, the mean MISDR is 0.70% and 2.1%, respectively. Frames retrofitted with the SD and HD, both the dampers satisfy the target performance. The seismic performance evaluation shows that response of frame retrofitted with the HD has improved significantly, reducing the residual deformation, MIDR, and

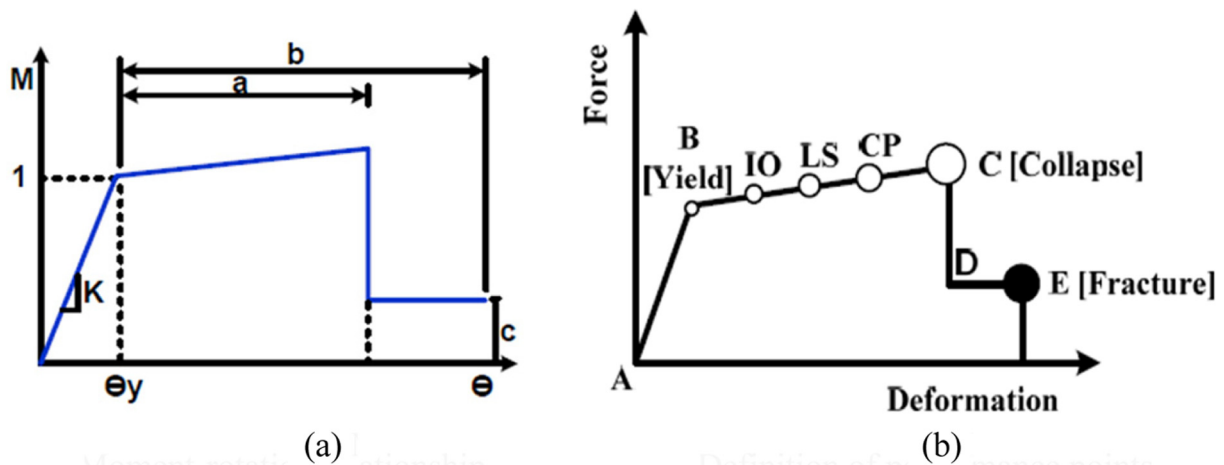


Figure 7. Nonlinear modeling of flexural members: (a) moment–rotation relationship and (b) definition of performance points.

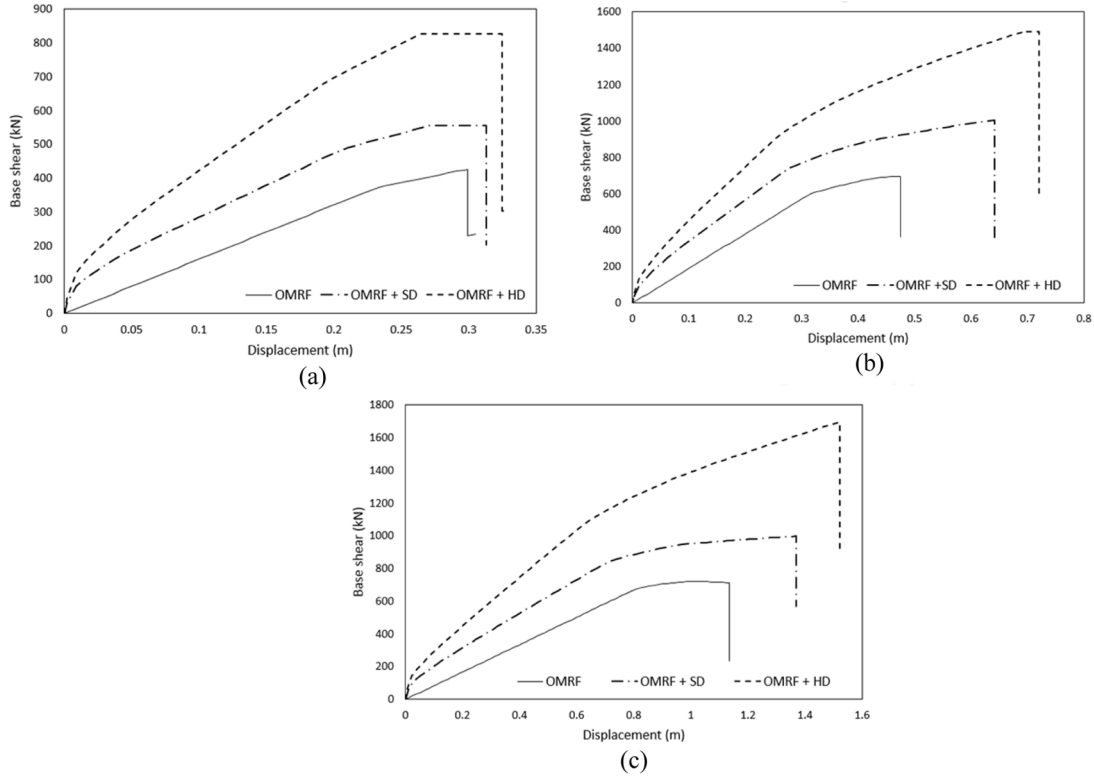


Figure 8. Nonlinear pushover curves of the bare frame (BF) and frame with SD and frame with HD: (a) three-story model, (b) five-story model, and (c) eight-story model.

Table 2. Earthquake records used for dynamic analysis.

ID no.	Record no.	Earthquake name	Component	PGA max. (g)
1	174	Imperial Valley	IMPVALL/H-EII230	0.38
2	68	San Fernando	SFERN/PELI80	0.21
3	138	Tabas	RSNI 138/TABAS-BOS	0.34

PGA: peak ground acceleration.

maximum displacement to meet the target performance of 1.0% MIDR at the design basis level of earthquake.

Fragility curve and AFC

Seismic fragility curves show the probability of a system reaching a limit state as a function of a seismic intensity measure such as spectral acceleration, and the seismic fragility is obtained from the results of the incremental dynamic analysis. Fragility is described by the conditional probability that the structural capacity C fails to resist the structural demand D . It is generally modeled as a log-normal cumulative density function (Cornell et al., 2002) given by

$$\begin{aligned}
 P[C < D | SI = x] &= 1 - \Phi \left[\frac{\ln(\hat{C}/\hat{D})}{\sqrt{\beta_{D/SI}^2 + \beta_C^2 + \beta_M^2}} \right] \\
 &= 1 - \Phi \left[\frac{\ln(\hat{C}/\hat{D})}{\beta_{TOT}} \right]
 \end{aligned} \quad (5)$$

where $\Phi[\cdot]$ is the standard normal probability integral, \hat{C} is the median structural capacity associated with a limit state, \hat{D} is the median structural demand, and β_C is system collapse uncertainty, uncertainty in the structural demand $\beta_{D/SI}$ and modeling uncertainties β_M . In this study, the total system collapse uncertainty β_{TOT} is assumed to be 0.6 throughout this study.

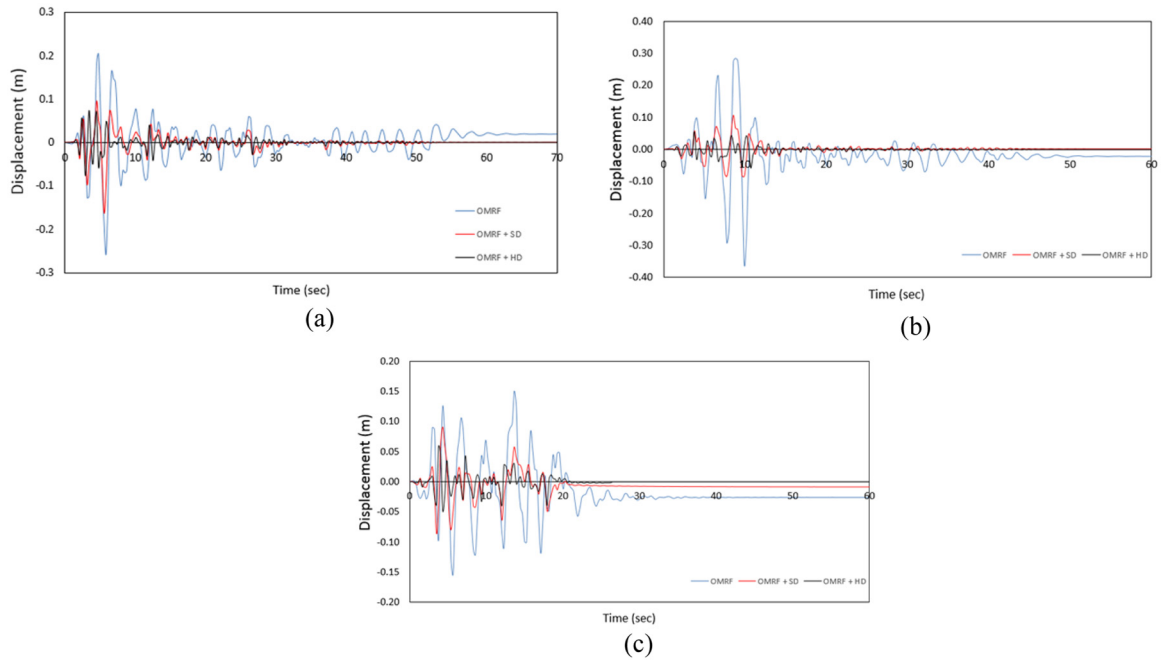


Figure 9. Roof displacement time history of five-story frame subjected to three earthquakes: (a) Imperial Valley, (b) San Fernando, and (c) Tabas.

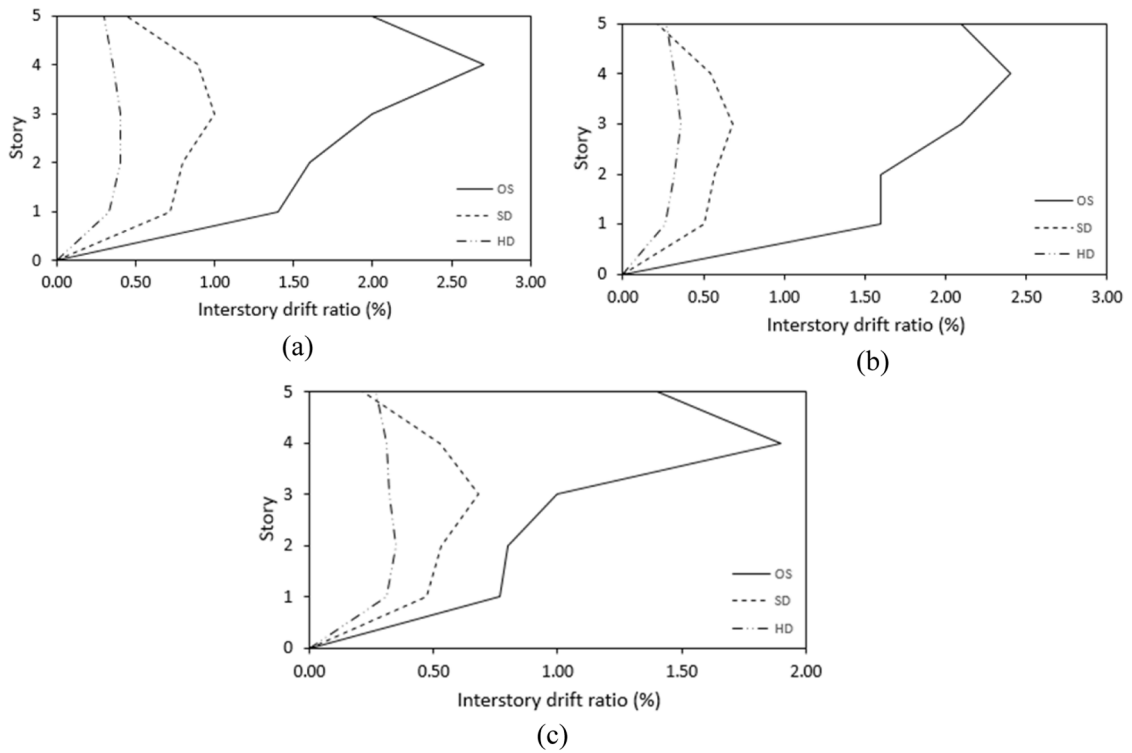


Figure 10. Maximum interstory drift ratios of the frame structures subjected to three earthquakes: (a) Imperial Valley, (b) San Fernando, and (c) Tabas.

Seismic hazard and earthquake ground motions

Site-specific hazard curve represents the annual frequency of exceedance of earthquakes with various peak ground accelerations. Uniform hazard spectra (UHS) are obtained from probabilistic seismic hazard analysis to characterize the seismic hazard for the selected site. The UHS used in this study are obtained from the 2014 national seismic hazard mapping developed by the U.S. Geological Survey. A site at the county of Los Angeles with soil type D is selected and the site-specific seismic hazard is derived. The site-specific hazard curve and the UHS for earthquakes with three different return periods (75, 500, and 2500 years) are constructed using the online tool provided by USGS (Geohazards, 2012) and are shown in Figure 11(a) and (b), respectively. The earthquakes with those return periods correspond to the seismic hazards associated with the three structural limit states, IO, LS, and CP, respectively. Thirty earthquake records are selected from the Pacific Earthquake Engineering Research (PEER) NGA database (PEER) for statistical analysis of the model structures. In the current study, spectrum matching is used to make the geometric mean of the acceleration response spectra of the records compatible with each hazard level peak ground acceleration, as shown in Figure 12. The scaling factors in the range of 1–4 are used to preserve the fundamental seismological features of the records after scaling (Hancock et al., 2008).

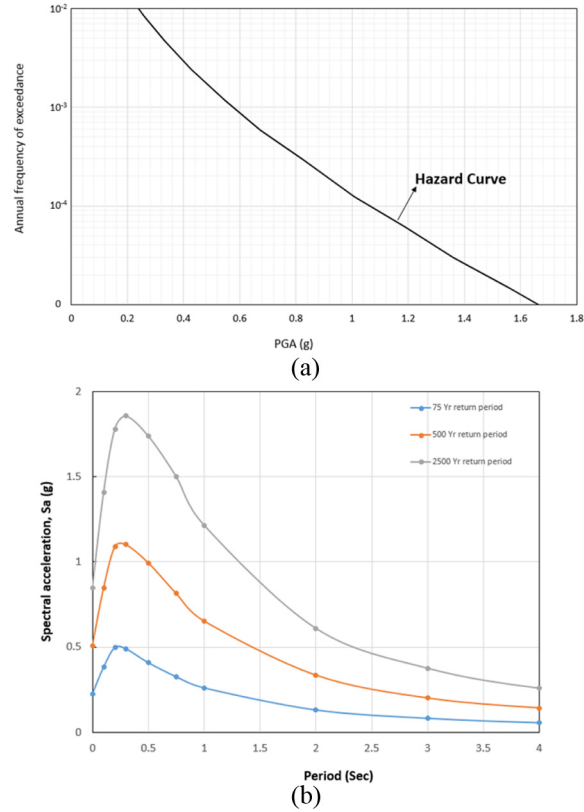


Figure 11. Seismic hazard curve and uniform hazard spectra (UHS) used in the analysis: (a) seismic hazard curve of Los Angeles and (b) UHS with 75-, 500-, and 2500-year return periods.

Results and observations

Based on the incremental dynamic analysis results, probabilities of reaching the limit states which are comprehensively defined in FEMA 356 are computed,

and these limit states are IO, LS, and CP, corresponding to the MIDR of 1%, 1.5%, and 2%, respectively. The service life of the model structure is assumed to be 50 years.

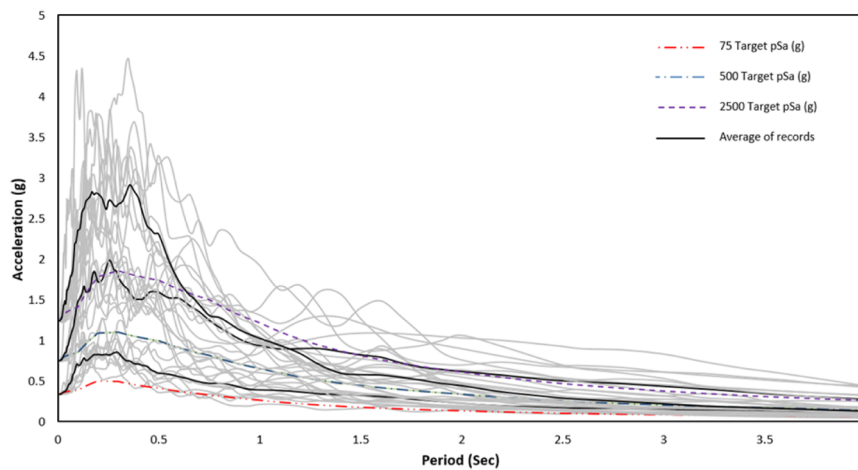


Figure 12. Response spectra of ground motions and their geometric mean scaled to PGA of UHS with 75-, 500-, and 2500-year return periods.

Fragility analysis generally requires a lot of non-linear dynamic analyses of structures using many earthquake records, which makes it difficult to apply the technique in structural engineering practice. In this study, simplified techniques are applied to significantly reduce the time and effort required for fragility analysis. The first step of the simplification is to transform the model structure into an equivalent single-degree-of-freedom (SDOF) system. For the conversion of the model structures to SDOF systems, it is assumed that the response of the structure is dominated by the fundamental vibration mode. Pushover analysis is used to obtain the structure capacity curve, which is transformed into the force–displacement relationship of the equivalent single degree of freedom (ESDOF) system. The details of the multi-degrees of freedom (MDOF) system to SDOF system transformation can be found in Qi and Moehle (1991), Kuramoto et al. (2000), and Jeong and Elnashai (2007).

Another simplification applied in this study is to use simplified fragility curve. In this step, the median drift capacity intensity S_a^c , the intensity measure that corresponds to the probability of exceedance equal to 50% of a specific limit state, is estimated using the AFC obtained using only two or three pairs of $(S_a, P(Ls_{S_a}))$ data, as shown schematically in Figure 13, instead of full fragility curve. The use of linear AFC is based on the observation that the slope of a fragility curve is nearly constant around the median capacity point. To draw a linear fragility curve, it is required to make a curve fitting for two or three points to predict the location of $P(Ls_{S_a}) = 50\%$ on the plot. If the probability of exceedance is too small, that is, less than 50%, then the return period of the selected hazard should be increased until the $P(Ls_{S_a})$ get closer to 50% or exceed it. On the other hand, if the probability of exceedance is too large, that is, less than 50%, then the return period of the selected hazard should be decreased until the $P(Ls_{S_a})$ get closer to 50% or less. Based on that, two pairs of $(S_a, P(Ls_{S_a}))$ data will be enough to draw the AFC.

From the figure, one can obtain the spectral acceleration corresponding to the median drift capacity (i.e. S_a^c). This spectral acceleration can be found easily by interpolation among the points used for constructing the AFC. Figure 14 and Table 3 compare the fragility analysis results of the five-story model structure with and without dampers obtained from the rigorous method and the approximate method.

It can be observed in the fragility curves that the frame retrofitted with HD has the least probability of reaching any limit states compared to the BF and frame retrofitted with SD. It can be observed that the difference between the approximate and rigorous fragility curves in S_a^c at 50% probability is 0.02 and 0.03 g

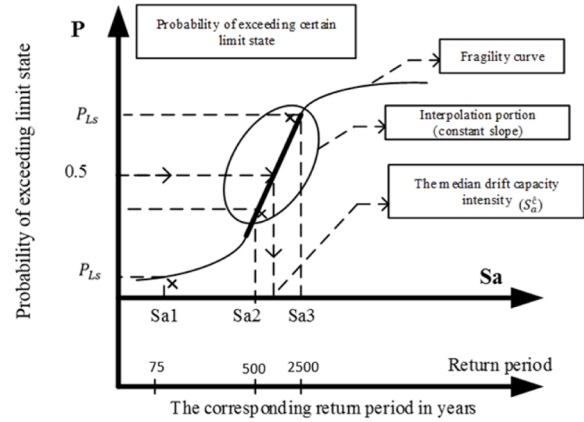


Figure 13. Schematic diagram for finding median capacity intensity using approximate fragility curve.

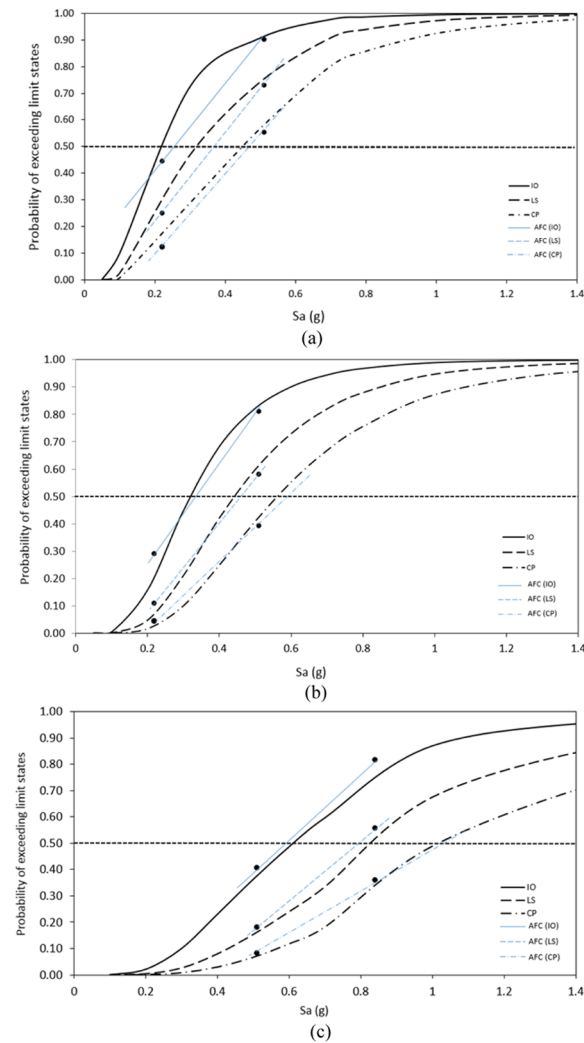


Figure 14. Full and approximate fragility curves for five-story model structures at three limit states: (a) original model, (b) model with slit dampers, and (c) model with hybrid dampers.

Table 3. Comparison of S_a^c obtained from full and approximate analyses of the five-story structures.

Model	Full fragility analysis			Approximate analysis		
	IO	LS	CP	IO	LS	CP
Original model	0.22	0.32	0.45	0.24	0.35	0.45
Model with SD	0.32	0.44	0.56	0.33	0.45	0.59
Model with HD	0.61	0.82	1.0	0.57	0.80	1.03

HD: hybrid damper; IO: immediate occupancy; LS: life safety; CP: collapse prevention; SD: slit damper.

for IO and LS damage states, respectively, for the BF. In the frame equipped with SD, the difference is 0.01 g for IO and LS states, but is increased to 0.03 g for CP state. The discrepancy for the frame with HD is 0.04, 0.02, and 0.03 g for IO, LS, and CP states, respectively, as observed in Figure 14. The discrepancies are contributed largely from the inadequate nonlinear behavior of the SDOF systems in comparison with the MDOF system models. However, the differences in S_a^c are not significant compared with the overall amplitude of the median capacity, and the approximate method seems to be valid to predict the location of $P(Ls_{Sa}) = 50\%$ on the fragility curve.

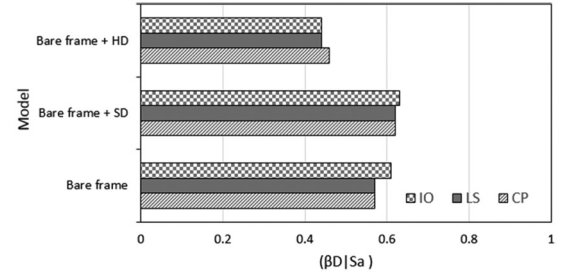
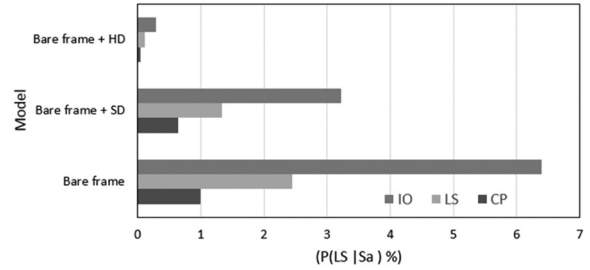
Expected LCC evaluation

To compute the damage cost of a structure subjected to a seismic load, the damage state probability, the annual probability of exceeding a selected limit state, needs to be obtained. Cornell et al. (2002) provide the following equation to compute the damage state probability P_{Ls}

$$P_{Ls} = H(S_a^c) \exp \left[\frac{1}{2} \frac{k^2}{b^2} (\beta_{D_{S_a}}^2 + \beta_C^2) \right] \quad (6)$$

where S_a^c is the spectral acceleration corresponding to the median drift capacity obtained from the AFC; $H(S_a^c)$ is the annual probability of exceedance at intensity S_a for a given site; k and b are the linear regression coefficients of hazard and drift demand on intensity S_a in logarithmic space; $\beta_{D_{S_a}}$ is the dispersion measure for drift demand D at given S_a ; and β_C is the dispersion measure for drift capacity C ((standard deviation of natural logarithm) assumed to be 0.3 based on previous studies (Cornell et al., 2002). Figure 15 depicts the drift demand dispersion and Figure 16 shows the annual probability of each damage state for the five-story model structure corresponding to the limit states.

With the damage state probabilities computed, the expected LCC of a structure can be calculated as follows (Wen and Kang, 2001)

**Figure 15.** Drift demand dispersion of five-story model structure corresponding to the limit states.**Figure 16.** Damage state probability for five-story model structure.

$$E[V_{Lc}] = V_o + \int_0^L E[V_{SD}] \left(\frac{1}{1 + \lambda} \right)^t dt = V_o + \alpha L E[V_{SD}] \quad (7)$$

where V_o is the initial construction cost, L is the service life of the structure, λ is the annual discount rate, and $E[V_{SD}]$ is the annual expected seismic damage cost which is governed by a Poisson process and does not depend on time. It is assumed that structural capacity does not degrade over time and the structure is restored to its original condition after each hazard. The parameters α , q , and $E[V_{SD}]$ can be formulated as

$$\alpha = [1 - \exp(-ql)]/ql \quad (8)$$

$$q = \ln(1 + l) \quad (9)$$

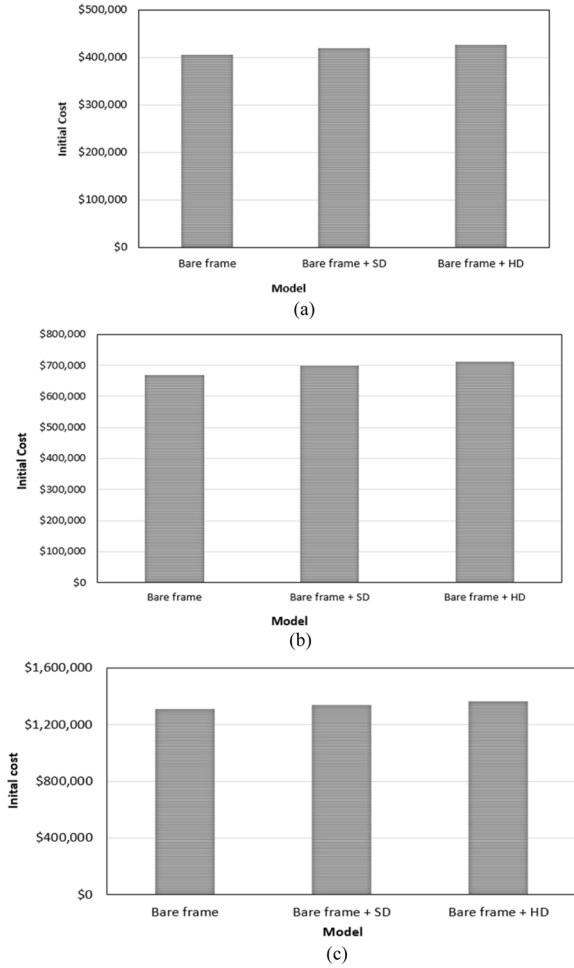


Figure 17. Initial cost of the model structures: (a) three-story model structures, (b) five-story model structures, and (c) eight-story model structures.

$$E[V_s D] = \sum_{i=1}^N V_i P_i \quad (10)$$

where N is the total number of limit states considered, P_i is the total probability that the structure is in the i th damage state throughout its lifetime, and V_i is the corresponding cost (which includes the cost of damage and its repair). In accordance with the definition of seismic hazard, three structural damage states are used (i.e. N is equal to 3) such as IO, LS, and CP, and V_i is assumed to be 30, 70 and 100%, respectively, of the initial cost of the structure (Fragiadakis et al., 2006). This implies that the damage cost is estimated based only on the interstory drift of the model structures. Even though damage cost will also depend on other factors such as residual displacement, their effects are not considered in this study. P_i is given by equation (11)

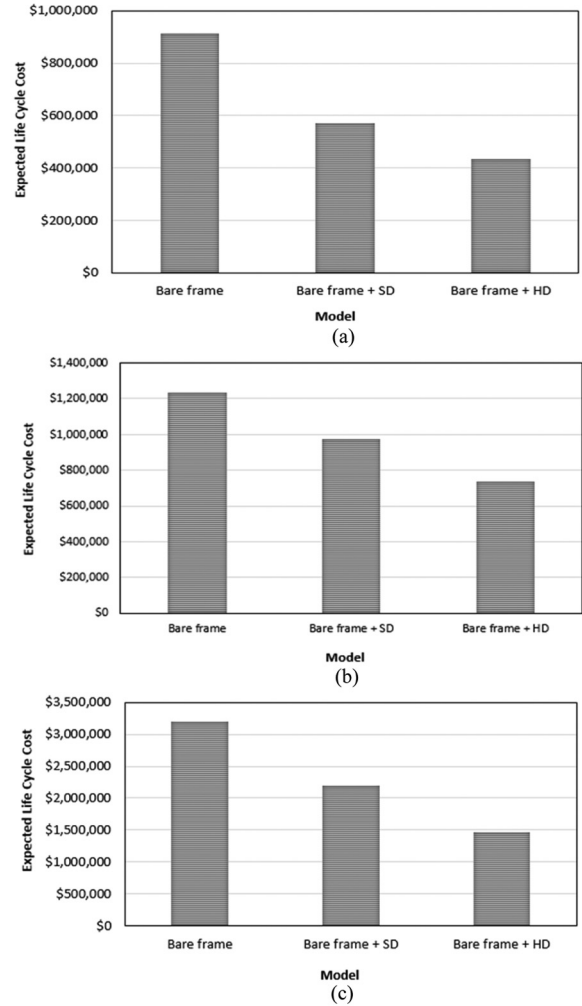


Figure 18. Expected life-cycle cost of the model structures: (a) three-story structures, (b) five-story structures, and (c) eight-story structures.

$$P_i = P(\Delta_D > \Delta_{C,i}) - P(\Delta_D > \Delta_{C,i+1}) \quad (11)$$

where Δ_D is the earthquake demand and $\Delta_{C,i}$ is the structural capacity, usually represented in terms of drift ratio, defining the i th damage state. The probability of demand greater than capacity, $\delta_D > \delta_{C,i}$ is evaluated as discussed in the previous step.

Figures 17 and 18 depict the initial and the expected LCC of the model structures for 30-year life span obtained from the simplified procedure described above. It is assumed that the unit costs of the slit and the HD are US\$2000 and US\$4000, respectively, including the installation and labor costs. It can be observed that the expected LCC of the structure retrofitted with the HDs is smallest, even though the initial cost is highest. The cost of structural steel is assumed to be US\$1,275/m³. It is observed that the initial cost

Table 4. Parameters used in LCC estimation of the five-story structures with HD.

Methods	Rigorous			Approximate		
	IO	LS	CP	IO	LS	CP
Limit state						
S_A^C (g)	0.61	0.82	1.0	0.57	0.80	1.03
$\beta_{D S_a}$	0.43	0.44	0.46	0.40	0.43	0.49
$H(S_a)$	0.0008	0.0003	0.0001	0.0010252	0.000327	0.000111
k_o	0.0002			0.0002		
k	2.75			2.75		
b	0.91			0.82		
β_C	0.3			0.3		
$P(L_{s s_a})$ %	0.29	0.11	0.05	0.42	0.15	0.07
P_i (%)	0.18	0.06	0.05	0.26	0.08	0.07
(LCC - V_o) (US\$)	25,609			30,051		
LCC (US\$)	734,000			739,000		
Difference	0.7%					

LCC: life-cycle cost; HD: hybrid damper; IO: immediate occupancy; LS: life safety; CP: collapse prevention.

of the structures with HD is only slightly higher than that of the original structure; however, the LCC is only 60.5% of the original structure. It is also observed that the addition of SMA bars to the SDs reduces the LCC of the model structures by 21%–26% for three-story, five-story, and eight-story frame.

Table 4 shows that the parameters appearing in the LCC estimation of the five-story frame obtained from a simplified LCC method are compared with those obtained from a more rigorous method using full fragility curve. The difference in the expected LCC of the five-story BF, frame with SD, and frame with HD is 4.5%, 1.15%, and 1.0%, respectively. It is also observed that the percentage difference marginally increases with the increase in number of stories; the difference in the three-story model structure is 3.7%, 1.5%, and 0.6%, respectively, whereas for the eight-story model the difference is 11%, 7%, and 5% for the BF, frame with SD, and frame retrofitted with HD, respectively. It is also observed that as the seismic intensity increases, the difference between the two results also slightly increases. However, considering the reduced computation time and the simplicity of the approximate method, the results are quite satisfactory.

Conclusion

In this study, a HD was developed by incorporating SMA bars with steel slit plate to be used for seismic retrofit of structures. The seismic performance of the HD was compared with the BF and frame equipped with conventional SD. In this study, a hybrid damper (HD) was developed by incorporating SMA bars with steel slit plate to be used for seismic retrofit of structures. The seismic performance of the HD was compared with the bare frame (BF) and the frame equipped with

conventional slit dampers (SD). For simplification of the LCC evaluation process, the model structures were converted to the equivalent SDOF systems, and the simplified damage probability was calculated for each limit state. The proposed methodology was validated by comparing the results of LCC for three different models of steel frames with and without dampers. For simplification of the LCC evaluation process, the conversion of MDOF system to equivalent SDOF system is carried out and the simplified damage probability was calculated for each limit state. The proposed methodology was validated by comparing the results of LCC for three different models of steel frames with and without dampers.

Even though the initial cost of the retrofit scheme with HD was high as compared to that with SD due to the added SMA, the LCC of the frames retrofitted with HD turned out to be lower than those of the frames retrofitted with SDs for the 50 year expected life span. The HD was able to reduce the average LCC of the five-story model structure about 35.5% and 21% compared with those of the BF and the frame retrofitted with steel SD, respectively. The fragility analysis showed that the probability of reaching a given limit states was minimized by installing the HD. Based on the analysis results, it could be concluded that the application of SMA bars in steel plate SDs significantly enhances the seismic performance of the retrofitted structure. The discrepancy in the LCC between the simplified and rigorous methods ranged from 1% to 11% depending on the number of the story of the model structures. Considering the reduced computation time and efforts, the simplified method applied in this study turned out to be a convenient tool for LCC estimation of building structures with energy dissipation devices.

Declaration of Conflicting Interests

The author(s) declared no potential conflicts of interest with respect to the research, authorship, and/or publication of this article.

Funding

The author(s) disclosed receipt of the following financial support for the research, authorship, and/or publication of this article: This research was supported by a grant (17CTAP-C132889-01) from Technology Advancement Research Program (TARP) funded by Ministry of Land, Infrastructure and Transport of Korean government.

References

- Chan RW and Albermani F (2008) Experimental study of steel slit damper for passive energy dissipation. *Engineering Structures* 30(4): 1058–1066.
- Computer and Structure Inc. (2010) *Analysis Reference Manual*. Berkeley, CA: Computer and Structure Inc.
- Cornell CA, Jalayer F, Hamburger RO, et al. (2002) Probabilistic basis for 2000 SAC federal emergency management agency steel moment frame guidelines. *Journal of Structural Engineering* 128(4): 526–533.
- FEMA 356 (2000) *Prestandard and Commentary for the Seismic Rehabilitation of Buildings*. Washington, DC: Federal Emergency Management Agency.
- Fragiadakis M, Lagaros ND and Papadrakakis M (2006) Performance-based multiobjective optimum design of steel structures considering life-cycle cost. *Structural and Multidisciplinary Optimization* 32(1): 1–11.
- Gencturk B (2013) Life-cycle cost assessment of RC and ECC frames using structural optimization. *Earthquake Engineering & Structural Dynamics* 42(1): 61–79.
- Geohazards (2012) <https://earthquake.usgs.gov/hazards/interactive/> (accessed 15 April 2017).
- Han Y, Yin H, Xiao E, et al. (2006) A kind of NiTi-wire shape memory alloy damper to simultaneously damp tension, compression and torsion. *Structural Engineering and Mechanics* 22(2): 241–262.
- Hancock J, Bommer JJ and Stafford PJ (2008) Numbers of scaled and matched accelerograms required for inelastic dynamic analyses. *Earthquake Engineering & Structural Dynamics* 37(14): 1585–1607.
- Jalaeefar A and Asgarian B (2014) A simple hybrid damping device with energy-dissipating and re-centering characteristics for special structures. *Structural Design of Tall and Special Buildings* 23(7): 483–499.
- Jeong S-H and Elnashai AS (2007) Probabilistic fragility analysis parameterized by fundamental response quantities. *Engineering Structures* 29(6): 1238–1251.
- Kim J and Shin H (2017) Seismic loss assessment of a structure retrofitted with slit-friction hybrid dampers. *Engineering Structures* 130: 336–350.
- Kuramoto HM, Teshigawara T, Okuzono N, et al. (2000) Predicting the earthquake response of buildings using equivalent single degree of freedom system. In: *Proceedings of the twentieth world conference on earthquake engineering*. Available at: <http://www.iitk.ac.in/nicee/wcee/article/1039.pdf>
- Lee J and Kim J (2015) Seismic performance evaluation of moment frames with slit-friction hybrid dampers. *Earthquakes and Structures* 9(6): 1291–1311.
- Li G, Zhang D and Yue Q (2009) Minimum life-cycle cost design of ice-resistant offshore platforms. *Structural Engineering and Mechanics* 31(1): 11–24.
- Ma H and Cho C (2008) Feasibility study on a superelastic SMA damper with re-centring capability. *Materials Science and Engineering* 473(1): 290–296.
- McCormick J, DesRoches R and Fugazza D (2007) Seismic assessment of concentrically braced steel frames with shape memory alloy braces. *Journal of Structural Engineering* 133(6): 862–870.
- Marshall JD and Charney FA (2012) Seismic response of steel frame structures with hybrid passive control systems. *Earthquake Engineering & Structural Dynamics* 41(4): 715–733.
- Miller DJ, Fahnestock LA and Eatherton MR (2012) Development and experimental validation of a nickel–titanium shape memory alloy self-centering buckling-restrained brace. *Engineering Structures* 40: 288–298.
- Mirtaheri M, Amini M and Khorshidi H (2017) Incremental dynamic analyses of concrete buildings reinforced with shape memory alloy. *Steel and Composite Structures* 23(1): 95–105.
- Naem A, NourEldin M, Kim J, et al. (2017) Seismic performance evaluation of a structure retrofitted using steel slit dampers with shape memory alloy bars. *International Journal of Steel Structures* 17(4): 1627–1638.
- Nakshatharan SS, Dhanalakshmi K and Ruth DJS (2014) Servo control of an under actuated system using antagonistic shape memory alloy. *Smart Structures and Systems* 14(4): 643–658.
- NourEldin M and Kim J (2016) Sensitivity analysis on seismic life-cycle cost of a fixed-steel offshore platform structure. *Ocean Engineering* 121: 323–340.
- NourEldin M, Kim M and Kim J (2017) Optimum distribution of steel plate slit dampers for seismic retrofit of building structures. *Submitted to Steel and Composite Structures* 25(4): 473–483.
- Ocel J, DesRoches R, Leon RT, et al. (2004) Steel beam-column connections using shape memory alloys. *Journal of Structural Engineering* 130(5): 732–740.
- Ozbulut OE and Silwal B (2016) Performance assessment of buildings isolated with S-FBI system under near-fault earthquakes. *Smart Structures and Systems* 17(5): 709–724.
- Pong W, Tsai C, Chen CS, et al. (2002) Parametric study for buildings with combined displacement-dependent and velocity-dependent energy dissipation devices. *Structural Engineering and Mechanics* 14(1): 85–98.
- Qi X and Moehle JP (1991) *Displacement Design Approach for Reinforced Concrete Structures Subjected to Earthquakes*. Berkeley, CA: Earthquake Engineering Research Center, College of Engineering, University of California.

- Qiu CX and Zhu S (2017) Shake table test and numerical study of self-centering steel frame with SMA braces. *Earthquake Engineering & Structural Dynamics* 46(1): 117–137.
- Rameshwar SI (2014) Rehabilitation of buildings and bridges by using shape memory alloys (SMA). *International Journal of Civil Engineering Research* 5(2): 163–168.
- Saffari H, Hedayat AA and Nejad MP (2013) Post-Northridge connections with slit dampers to enhance strength and ductility. *Journal of Constructional Steel Research* 80: 138–152.
- Salari N and Asgarian B (2015) Seismic response of steel braced frames equipped with shape memory alloy-based hybrid devices. *Structural Engineering and Mechanics* 53(5): 1031–1049.
- Shin H and Singh M (2014) Minimum failure cost-based energy dissipation system designs for buildings in three seismic regions—part I: elements of failure cost analysis. *Engineering Structures* 74: 266–274.
- Sullivan TJ, Welch DP and Calvi GM (2014) Simplified seismic performance assessment and implications for seismic design. *Earthquake Engineering & Engineering Vibration* 13(1): 95–122.
- Taflanidis A and Gidaris I (2013) Life-cycle cost based optimal retrofitting of structures by fluid dampers. *Structures Congress 2013*: 1777–1788.
- Torra V, Carreras G, Casciati S, et al. (2014) On the NiTi wires in dampers for stayed cables. *Smart Structures and Systems* 13(3): 353–374.
- Tsai C, Chen K and Chen C (1998) Seismic resistibility of high-rise buildings with combined velocity-dependent and velocity-independent devices. *American Society of Mechanical Engineers* 366: 103–110.
- Uetani K, Tsuji M and Takewaki I (2003) Application of an optimum design method to practical building frames with viscous dampers and hysteretic dampers. *Engineering Structures* 25(5): 579–592.
- Wen YK, Kang YJ (2001) Minimum building life cycle cost design criteria I: Methodology. *Journal of Structural Engineering (ASCE)*; 127(3): 330–337.
- Wierschem N and Andrawes B (2010) Superelastic SMA–FRP composite reinforcement for concrete structures. *Smart Materials and Structures* 19(2): 025011.
- Zhu S and Zhang Y (2008) Seismic analysis of concentrically braced frame systems with self-centering friction damping braces. *Journal of Structural Engineering* 134(1): 121–131.